Speed Control of Interior Permanent Magnet Synchronous Motor Drive for the Flux Weakening Operation

Jang-Mok Kim, *Student Member, IEEE,* and Seung-Ki Sul, *Member, IEEE*

Abstract— **A novel flux-weakening scheme for the interior permanent magnet synchronous motor (IPMSM) is proposed. This is implemented based on the output of the synchronous PI current regulator-reference voltage to the PWM inverter. The onset of flux weakening and the flux level are adjusted inherently by the outer voltage regulation loop to prevent saturation of the current regulator. Attractive features of this flux weakening scheme include no dependency on the machine parameters, the guarantee of current regulation at any operating condition, and smooth and fast transition into and out of the flux weakening mode. Experimental results at various operating conditions including the case of detuned parameters are presented to verify the feasibility of the proposed control scheme.**

Index Terms—**Flux weakening, IPMSM, outer voltage regulation loop.**

I. Introduction

THE interior permanent magnet synchronous motor (IPMSM) has gained an increasing popularity in recent years for a wide variety of industrial drive applications. The magnets are buried inside the rotor core with a steel pole piece in the IPMSM. Because of this geometry, IPMSM has a mechanically robust rotor construction, a rotor saliency, and the low effective airgap. These features permit this machine to be operated not only in the constant torque region but also in the constant power region up to a high speed by flux weakening [1], [3].

Recently some algorithms for flux weakening have been published for IPMSM [3], [5]–[7]. A six-step voltage control scheme in constant power region was proposed [5]. This scheme does not depend on the machine parameters, impress six-step voltage for the flux weakening operation, and thus gives maximum utilization of the dc link voltage. However, in order to change the control mode from the constant power mode to the constant torque mode, the information of the flux linkage is required. On the other hand, there was an attempt to utilize the feedforward flux weakening scheme [6]. But in this scheme, all machine parameters are needed to regulate the machine current in the flux weakening region. In [7] a voltage compensator and a current regulator with feedforward decoupling controller were proposed for the flux weakening operation. This voltage compensator operates well in tuned operating conditions. But if there is an extra voltage margin due to the weakening of the permanent magnet flux linkage according to temperature rise or dc link voltage variations, the drive system may diverge because of an improper operation of the voltage compensator.

In previous studies the performance of IPMSM drive system in an extended speed region was strongly dependent on the motor parameters because the model of IPMSM, especially the stator voltage equation of the motor, is basically used for the flux weakening control. Unfortunately, the flux linkage of permanent magnet and the stator resistance of the motor vary according to the temperature [8]. Moreover, the d-axis and q-axis self-inductance, L_{ds}, L_{qs}, vary with the airgap flux [9]. In the constant torque region an improper tuning of parameters of the IPMSM drive may result in only a small reduced torque and a small degradation of the efficiency of the machine because IPMSM is controlled by the maximum torque per ampere control based on the model of the machine. But in the flux weakening operation region an improper tuning of parameters of the IPMSM drive may result in a reduced torque capability and stability problems in flux weakening operation.

In this paper, a novel flux weakening control scheme is described. The inverter output voltage, which is the output of the current regulator, is controlled up to the maximum available value related to the dc link voltage by the outer voltage regulating loop. The onset of flux weakening and the level of the flux are adjusted inherently with the voltage regulating loop. This scheme does not depend on the model of IPMSM for the flux weakening control in contrast to the previous researches, but it depends on the basis of inverter output voltage regulation. An additional feature of this scheme is that the performance of the current regulator at any operating condition is guaranteed due to the antisaturation control of the regulator with the outer voltage feedback loop. The current regulator used in this study is a synchronous PI current regulator with feedforward decoupling loop [2], [6].

Experimental results for a laboratory IPMSM drive system under various operating conditions are presented to verify the feasibility of the proposed control scheme.

II. Modeling of IPMSM

The machine model for the IPMSM on the synchronously rotating d-q reference frame with an electrical angular velocity

Paper IPCSD 96-33, approved by the Industrial Drives Committee of the IEEE Industry Applications Society for presentation at the 1995 IEEE Industry Applications Society Annual Meeting, San Diego, CA, October 6–10. Manuscript released for publication May 13, 1996.

The authors are with the School of Electrical Engineering, Seoul National University, Seoul 151–742, Korea.

Publisher Item Identifier S 0093-9994(97)00987-0.

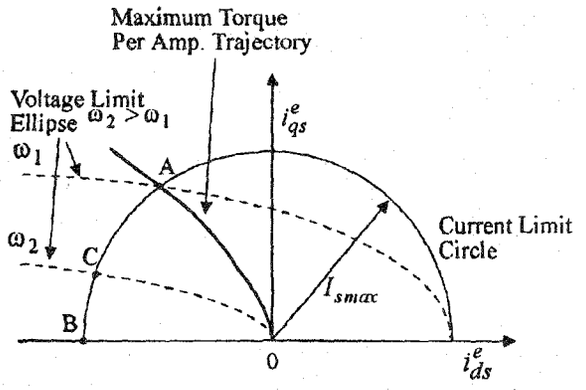

Fig. 1. The maximum torque-per-current trajectory in the plane.

ω_e can be represented in the matrix form as follows [1], [6], [7]:

$$\begin{bmatrix} V^e_{ds} \\ V^e_{qs} \end{bmatrix} = \begin{bmatrix} R_s & -\omega_e L_{qs} \\ \omega_e L_{ds} & R_s \end{bmatrix} \begin{bmatrix} i^e_{ds} \\ i^e_{qs} \end{bmatrix} + \begin{bmatrix} 0 \\ \omega_e \psi_f \end{bmatrix} \quad (1)$$

where the superscript e denotes the synchronous reference frame, and

V^e_{ds}, V^e_{qs} d-axis, q-axis stator voltage;
i^e_{ds}, i^e_{qs} d-axis, q-axis stator current;
L_{ds}, L_{qs} d-axis, q-axis stator self-inductance;
R_s stator resistance;
ψ_f per phase magnetic flux linkage

and the developed torque equation of IPMSM is expressed as follows:

$$T_e = \tfrac{3}{2}[\psi_f i^e_{qs} + (L_{ds} - L_{qs}) i^e_{qs} i^e_{ds}] \quad (2)$$

where p is the number of pole pairs.

As shown in (2), the electrical torque consists of the magnetic alignment torque produced by the flux linkage and the reluctance torque produced by the saliency ($L_{qs} > L_{ds}$). This feature is an inherent characteristic of this type machine, while only the magnet alignment torque is produced in the different type machine such as the surface mount permanent magnet synchronous motor (SPMSM). Therefore, it is desirable that the reluctance torque should be properly utilized in order to increase the whole efficiency of the IPMSM drive.

In Fig. 1, the maximum torque-per-current trajectory on the synchronously rotating d–q reference current plane is illustrated. When the machine is operated from the start up to an angular speed ω_1 in the constant torque region in Fig. 1, the voltage limit ellipse exceeds the cross point A of the maximum torque-per-ampere trajectory and the maximum current boundary represented by $I_{s\max}$ which is determined by the current rating of the machine or the maximum current capability of the inverter. Hence, the voltage limitation is not needed to consider in this constant torque region. The stator d-axis and q-axis current is to be controlled to use the reluctance torque fully and to maximize the machine efficiency.

The magnitude of the output of the speed controller $|i^e_s|$ can be expressed as

$$|i^e_s| = \sqrt{i^{e2}_{qs} + i^{e2}_{ds}}. \quad (3)$$

From (2) and (3), the d–q axis components of the current vector for the maximum torque-per-ampere are derived as follows:

$$i^e_{qs} = \text{sign}\,(i^e_s) \cdot \sqrt{i^{e2}_s - i^{e2}_{ds}}$$

where

$$\begin{cases} \text{if} \quad i^e_s \geq 0, & \text{sign}(\text{i}^\text{e}_\text{s}) = 1 \\ \quad\; i^e_s < 0, & \text{sign}(\text{i}^\text{e}_\text{s}) = -1 \end{cases} \quad (4)$$

$$i^e_{ds} = \frac{\psi_f - \sqrt{\psi_f^2 + 8(L_{qs} - L_{ds})^2 i^{e2}_s}}{4(L_{qs} - L_{ds})}. \quad (5)$$

In the constant torque region, the locus of the current vector according to (4) and (5) is shown as a curve from point O to point A in Fig. 1.

III. Description of the Flux Weakening Control Scheme

A. Operating Limits in the Flux Weakening Region

The maximum voltage $V_{s\max}$ that the inverter can supply to the machine is limited by the dc link voltage and the PWM strategy. In this paper, a PWM strategy based on voltage space vector is used and $V_{s\max}$ is $V_{\text{dc}}/\sqrt{3}$ [3]. Also the maximum current $I_{s\max}$ is determined by the inverter current rating and machine thermal rating. Therefore, the voltage and current of the motor have the following limits [10]:

$$V^{e2}_{ds} + V^{e2}_{qs} \leq V^2_{s\max} \quad (6)$$

$$i^{e2}_{ds} + i^{e2}_{qs} \leq I^2_{s\max}. \quad (7)$$

B. Maximum Torque Operation in the Flux Weakening Region

The torque capability in the flux-weakening region is determined by both the voltage and the current limits. In this region, the synchronously rotating d–q reference frame currents i^e_{qs} and i^e_{ds} producing the maximum output torque become the values at the crossing point of the current limit circle and the voltage limit ellipse [6], [7], [9]. With the consideration of (6) and (7), i^e_{qs} and i^e_{ds} for maximum torque operation in the flux-weakening region can be modified as follows:

$$i^e_{qs} = \text{sign}\,(i^e_s) \cdot \sqrt{i^{e2}_s - i^{e2}_{ds}}$$

$$\begin{cases} \text{if} \quad i^e_s \geq 0, & \text{sign}(\text{i}^\text{e}_\text{s}) = 1 \\ \quad\; i^e_s < 0, & \text{sign}(\text{i}^\text{e}_\text{s}) = -1 \end{cases} \quad (8)$$

and (9), shown at the bottom of the next page, where

$$V_f = V_{s\max} - R_s I_{s\max}$$

In this region, the current vector trajectory should move along the boundary of the current limit circle ($A \rightarrow B$) in Fig. 1 as the rotor speed increases. In other words, the voltage limit ellipse scales inversely with speed so that increasing the speed produces a family of progressively smaller nested ellipses.

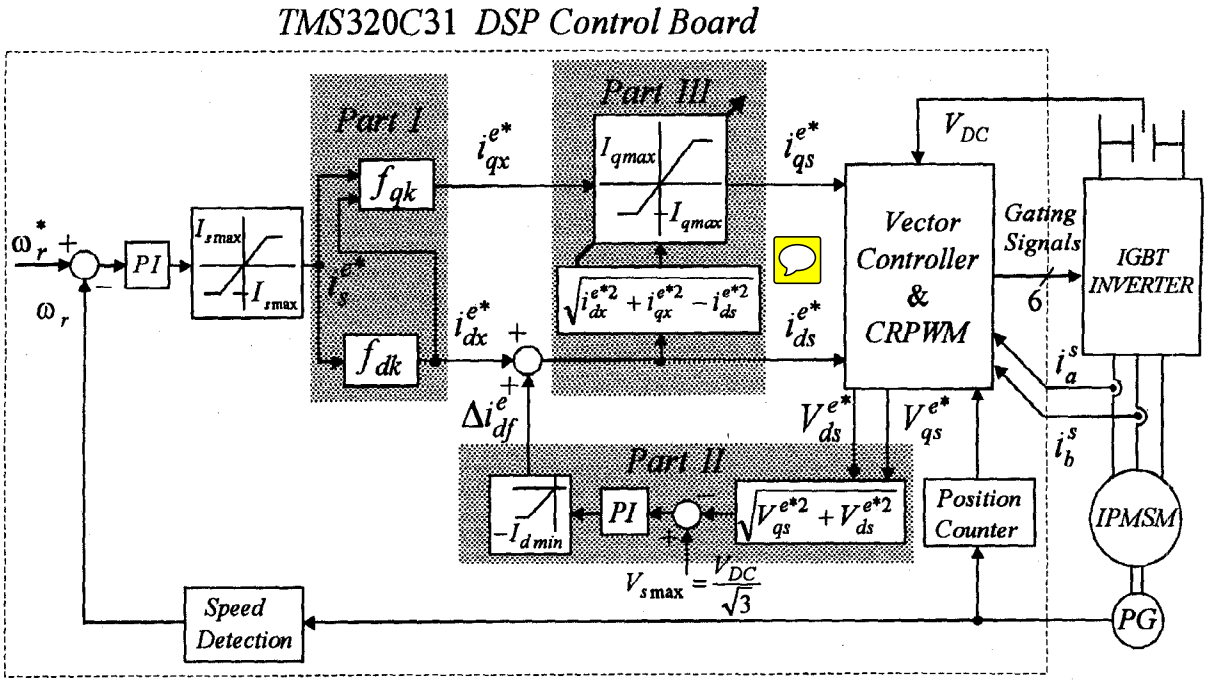

Fig. 2. Block diagram of IPMSM drive system.

Without a proper flux weakening operation, the current regulator would be saturated and lose its controllability at a higher speed. Since the onset of the current regulator saturation varies according to load condition and the machine parameters, the beginning point of flux weakening and the flux level should be changed. A late start of the flux weakening may result in undesired output torque drop according to the saturation of the current regulator, but an early start deteriorates the acceleration performance. Therefore, it is desirable to change the onset point of flux weakening according to load condition and the machine parameters. From (1) and (7), the optimal point can be deduced as follows:

$$\omega_{\text{base}} = \frac{-b + \sqrt{b^2 - 4ac}}{2a} \tag{10}$$

where

$$\begin{cases} a = (L_{qs} i^e_{qs})^2 + (L_{ds} i^e_{ds})^2 + \Psi_f^2 + 2L_{ds}\Psi_f i_{ds} \\ b = 2(L_{ds} - L_{qs}) R_s i^e_{ds} i^e_{qs} + 2R_s \Psi_f i^e_{qs} \\ c = R_s^2 (i^{e^2}_{ds} + i^{e^2}_{qs}) - V^2_{\text{smax}}. \end{cases}$$

In the high speed region the base speed ω_{base} is severely influenced by the permanent magnet flux linkage which varies with operating temperature and the q-axis inductance varies according to the amplitude of q-axis current.

C. Description and Features of the Proposed Scheme

Fig. 2 illustrates a block diagram of the speed control system implemented with the proposed flux weakening control algorithm. Part I is the torque controller in the constant torque operating mode. The current command $i_s^{e^*}$, which is the output of the PI speed controller, is decomposed into d- and q-axes components, $i_{dx}^{e^*}$ and $i_{qx}^{e^*}$, according to (4) and (5) along the maximum torque-per-ampere trajectory until the current regulator begins to saturate.

The proposed flux weakening controller can be divided to Parts II and III, as shown in Fig. 2. The main idea of the proposed flux weakening control algorithm is the use of the output reference voltage of the synchronous PI current regulator to identify the onset of the flux weakening. As the speed of the IPMSM is getting higher during acceleration, the output of the current regulator, especially the q-axis current regulator, increases and approaches to the boundary of the pulsewidth modulator. Without a proper counter measure, the performance of the current regulator gets worse due to the reduced margin of the voltage and finally it loses its controllability. As shown in Fig. 2, the controller in Part II ensures the margin of the voltage and increases the d-axis current toward the negative direction to prevent saturation of the current regulators. Thanks to this outer voltage regulating loop the flux level is inherently adjusted and the flux weakening operation is accomplished automatically. At the low and intermediate speed region, the magnitude of the output voltage of the current regulator $V_{qds}^{e^*} (= \sqrt{V_{ds}^{e^{*2}} + V_{qs}^{e^{*2}}})$ is usually less than V_{smax} and thus Part II is not activated. Even in this case, if the dc link voltage drops suddenly, the flux weakening

$$i^e_{ds} = \frac{L_{ds}\psi_f - \sqrt{(L_{ds}\Psi_f)^2 + (L_{qs}^2 - L_{ds}^2)(\Psi_f^2 + (L_{ds} i_s^e)^2 - (V_f/\omega_e)^2)}}{L_{qs}^2 - L_{ds}^2} \tag{9}$$

operation can be carried out autonomously. The incremental d-axis current Δi^e_{df} serves as the control input to the d-axis for flux weakening operation, and the limitation of Δi^e_{df} is designated as $I_{d\min} = I_{s\max} - I_{drate}$, where I_{drate} is the d-axis current at point A in Fig. 1.

The basic action of Part III is to depress the q-axis current command $i^{e^*}_{qx}$ in response to the presence of a growing d-axis current command $i^{e^*}_{ds}$, signifying current regulator saturation and asking for flux weakening operation.

By depressing the q-axis current command $i^{e^*}_{qx}$ in Part III and increasing d-axis current command $i^{e^*}_{ds}$ toward the negative direction in Part II at the same time, the current regulators are able to regain the practical ability of regulating of the d-axis and the q-axis current (i^e_{ds}, i^e_{qs}) along the crossing point of the current limit circle and voltage limit ellipse in the flux weakening operation. Under the limit of the voltage and current the maximum torque-per-ampere is produced at the crossing point of the current limit circle and voltage limit ellipse in the constant power region. And $I_{q\max}$ is determined from $i^{e^*}_{qx}, i^{e^*}_{ds}$ and Δi^e_{df} in Part III, as shown in Fig. 2. In the constant torque region, Part III is not activated because $i^{e^*}_{ds}$ equals $i^{e^*}_{dx}$, namely Δi^e_{df} is zero. If Part III is activated, the d- and q-axis current $(i^{e^*}_{ds}, i^{e^*}_{qs})$ vectors, which initially lies on the maximum torque-per-ampere locus and inside the voltage limit ellipse at a given speed (the segment: $0 \rightarrow A$), is forced to move along the boundary of the current limit circle $(A \rightarrow B)$ in Fig. 1 as the rotor speed increases. No additional feedback signal is required to implement the proposed flux weakening algorithm except the phase currents, the rotor position, V_{DC} and the speed feedback which is already available for the vector rotator and the speed control in the constructed system as shown in Fig. 2.

This scheme for flux weakening utilizes not the model of the IPMSM but the reference output voltage of the synchronous PI current regulator and the outer voltage regulating loop, and thus it is robust and insensitive to load condition and the machine parameters. The flux weakening algorithm described above is optimal in the sense of torque generation under the limit of current and voltage in overall operating speed range.

IV. Experimental Results

The system shown in Fig. 2 is implemented with a TMS320C31 DSP control board and a current regulated PWM IGBT inverter. The switching frequency of the inverter is 5 kHz and the space vector PWM algorithm is used for maximum utilization of the dc link voltage. The sampling time of the current regulation loop is 100 μ/s and that of the outer voltage regulating loop and speed control loop is 1 ms. The rotor position for the vector rotator and the rotor speed for the speed control are obtained with an encoder of 2500 pulses per revolution. The control algorithm including the proposed flux weakening scheme was fully implemented with software. The program was written in C language and the size is about 2K words.

When the speed reference changes from -2500 to 2500 r/m and again to -2500 r/m, four-quadrant operation of the drive system which includes transition between the constant torque and the constant power modes is shown in Fig. 3. The machine operates well with full performance in the constant torque region as well as in the constant power region in both directions of speed and torque. The transition between the constant torque region and the constant power region is fast and smooth at all conditions of operation. $\hat{V}^{e^*}_{qds}$ in Fig. 3(d) is the low-pass filtered output of reference voltage, $V^{e^*}_{qds}$. When $\hat{V}^{e^*}_{qds}$ reaches $V_{s\max}$, the flux weakening operation begins at this speed. The error between $V_{s\max}$ and $V^{e^*}_{qds}$ feeds the voltage regulating loop. The PI compensator increases d-axis current toward the negative direction to keep the current regulator from saturation, as shown in Fig. 3(c) and (e). The nominal machine parameters and inverter are shown in Table I.

The value of $V_{s\max}$ is set according to the dc link voltage. The nominal value of $V_{s\max}$ is about 150 V instead of the ideal value of 173 V at nominal dc link voltage 300 V. The voltage

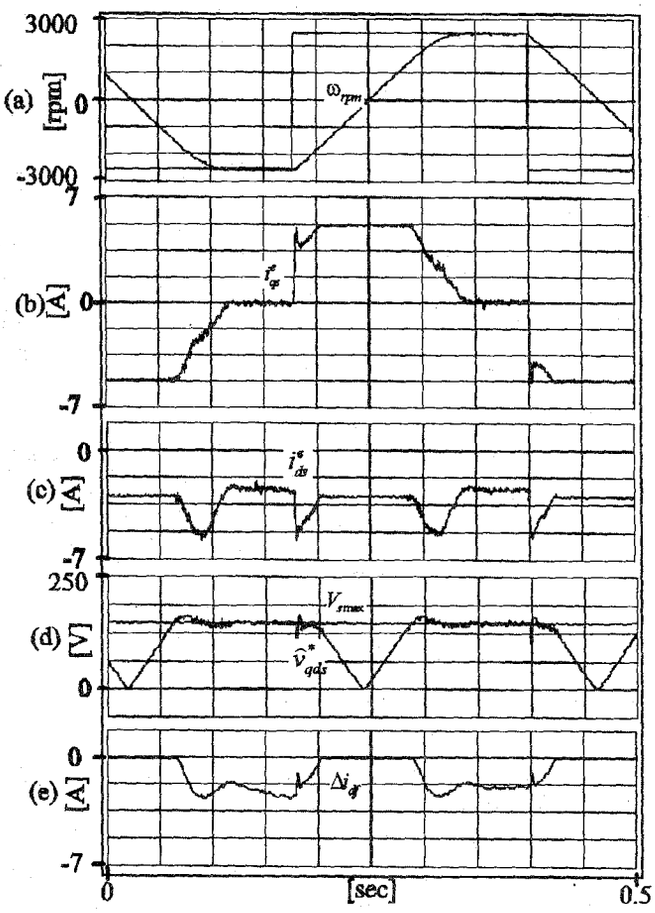

Fig. 3. Dynamic performance of the proposed scheme.

TABLE I
Nominal Parameters of IPMSM at 25°C

900[W], 220[V], 4[pole], 1700[rpm]
Rs : 4.3[Ω], Ψ_f : 0.272[Wb], L_{ds} : 27[mH]
L_{qs} : 67[mH], V_{DC}=300[V],
I_{rate}= 3[A], $I_{s\max} = 2I_{rate}$,
J=0.000179[$Kg\,m^2$] (motor and load inertia)

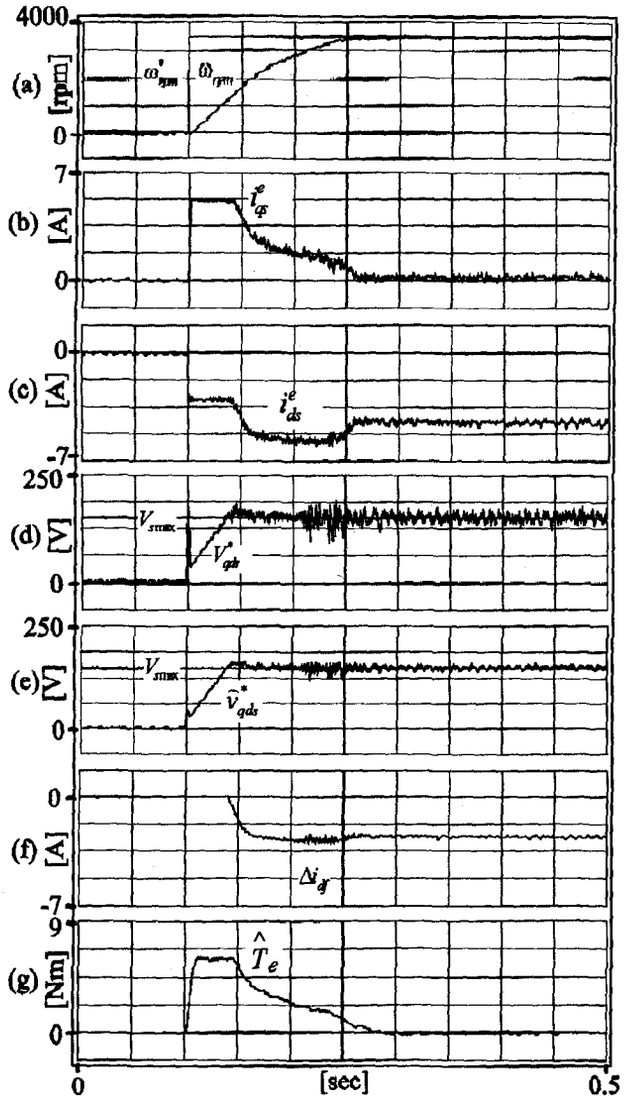

Fig. 4. In case of exactly tuned parameters at 25°C

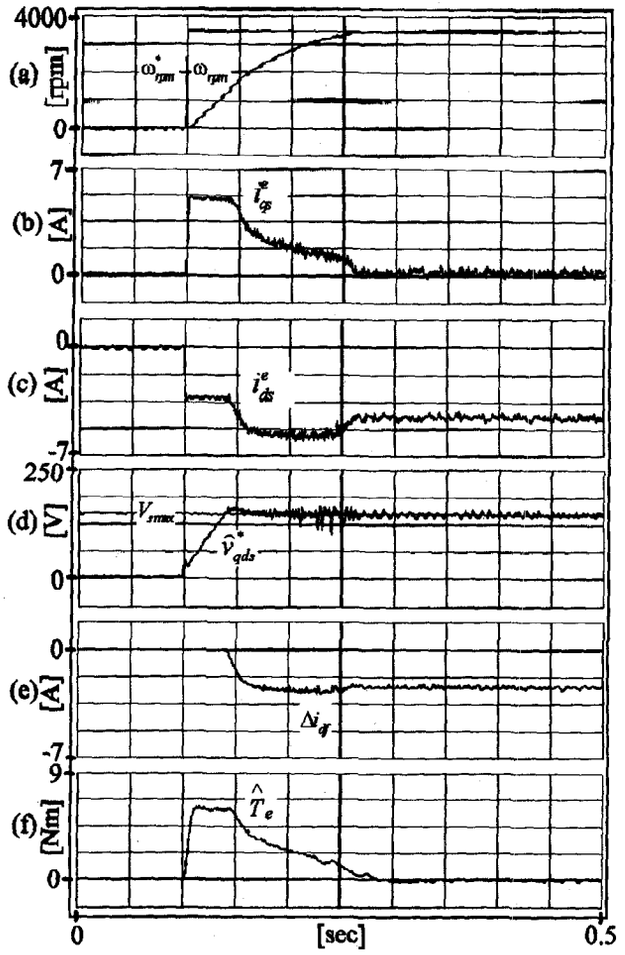

Fig. 5. In case of detuned parameters at 120°C.

difference can be explained as dead time effect, voltage drop of switching device, and the margin of the voltage for current forcing.

To show the operation in the extended speed region the speed command is changed from 0 to 3500 r/m in Fig. 4. The machine behaves well as expected. 3500 r/m is about twice the base speed. The unfiltered waveform of $V_{qds}^{e^*}$ is shown in Fig. 4(d), which is very sharp and fluctuating.

Fig. 5 shows the dynamic operation with the same condition as Fig. 4 except the machine parameters. The parameters are detuned from the nominal values to the values at 120 °C. The effect of the parameters is shown in the constant torque operation. By comparing the waveforms of the Fig. 4(a) and Fig. 5(a), the speed response of the case of the exactly tuned parameters and that of the detuned parameters is the same, and as shown from Fig. 4(g) and Fig. 5(f), the produced torques are also the same. These torques are estimated by using a method of observer [11], [12].

Therefore, it is clear that the performance of the flux weakening operation is irrespective to the variation of the machine parameters.

V. Conclusions

In this paper, a novel flux weakening control algorithm is proposed. The principal feature of the proposed flux weakening algorithm is use of the outer voltage regulating loop. The loop keeps the current controller from saturation by adjusting the flux level of the machine. Hence the onset of flux weakening and the regulation of the flux level is inherently achieved with the feedback of the output reference voltage of the current regulator. Other features of the proposed flux weakening control scheme are no requirement of additional hardware and robustness to the variation of the machine parameters. The experimental results clarify the effectiveness of the proposed scheme. It operates well with full performance not only in the constant torque region but also in the constant power region in both directions of speed and torque. The transition between the constant torque region and the constant power region is fast and smooth at all operating conditions irrespective of parameter detuning.

References

[1] T. M. Jahns, G. B. Kliman, and T. W. Neumann, "Interior permanent-magnet synchronous motors for adjustable-speed drive," *IEEE Trans. Ind. Applcat.*, vol. IA-22, pp. 738–747, July/Aug. 1986.

[2] T. M. Rowan and R. J. Kerkman, "A new synchronous current regulator and an analysis of current-regulated PWM inverters," *IEEE Trans. Ind. Applicat.*, vol. IA-22, pp. 678–690, July/Aug. 1986.

[3] T. M. Jahns, "Flux-weakening regime operation of an interior permanent-magnet synchronous motor drive," *IEEE Trans. Ind. Applicat.*, vol. IA-23, pp. 681–689, July/Aug. 1986.
[4] H. W. Van Der Broeck *et al.*, "Analysis and realization of a pulse-width modulator based on voltage space vectors," *IEEE Trans. Ind. Applicat.*, vol. 24, pp. 142–150, Jan./Feb. 1988.
[5] B. K. Bose, "A high-performance inverter-fed drive system of an interior permanent magnet synchronous machine", *IEEE Trans. Ind. Applicat.*, vol. 24, pp. 987–997, Sept./Oct. 1988.
[6] S. R. MacMinn and T. M. Jahns, "Control techniques for improved high-speed performance of interior pm synchronous motor drives," *IEEE Trans. Ind. Applicat.*, vol. 27, pp. 997–1004, Sep./Oct. 1991.
[7] S. Morimoto, M. Sanada, and Y. Taketa, "Wide-speed operation of interior permanent magnet synchronous motors with high-performance current regulator," *IEEE Trans. Ind. Applicat.*, vol. 30, pp. 920–926, July/Aug. 1994.
[8] T. Sebastian, "Temperature effects on torque production and efficiency of PM motors using NdFeB magnets," in *Proc. IEEE/IAS Conf. Rec.*, pp. 78–83, 1993.
[9] B. Sneyers, D. W. Novotny, and T. A. Lipo, "Field weakening in buried permanent magnet ac motor drives," *IEEE Trans. Ind. Applicat.*, vol. IA-21, pp. 398–407, Mar./Apr. 1991.
[10] Sang-Hoon Kim and Seung-Ki Sul, "Voltage control strategy for maximum torque operation of induction machine in the field weakening region," in *Proc. IECON'94*, pp. 599–604, 1994.
[11] V. R. Stefanovic and R. M. Nelms, "Microprocessor control of motor drives and power converters," in *Proc. IEEE/IAS Tutorial*, pp. 8-1–8-20, 1991.
[12] G. H. Hostetter, C. J. Savant Jr., and R. T. Stefani, *Design of Feedback Control Systems*, 2nd ed. Philadelphia: Saunders College, 1989.

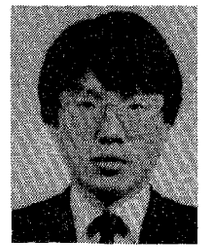

Jang-Mok Kim (S'94) was born in Pusan, Korea, in 1961. He received the B.S. degree from Pusan National University in 1988, and the M.S. degree from Seoul National University, Korea, in 1990, both in electrical engineering. He is presently working toward the Ph.D. degree at Seoul National University.

His research interests are in high-performance electric machine drives.

Seung-Ki Sul (S'78–M'87) was born in Pusan, Korea, in 1958. He received the B.S., M.S., and Ph.D. degrees in electrical engineering from Seoul National University, Seoul, Korea, in 1980, 1983, and 1986, respectively.

He was with the Department of Electrical and Computer Engineering, University of Wisconsin, Madison, as a Visiting Research Associate from 1986 to 1988. From 1988 to 1990 he was with GoldStar Industrial Systems Company, Seoul, as a principal research engineer. Since 1991, he has been with the Department of Electrical Engineering, Seoul National University. His present research interests are in high-performance electric machine control using power electronics. He is performing various research projects for industrial systems and some of the results are applied to the fields of industrial high-power electric machine control.